

Research on Detection Method for Tunnel Lining Defects Based on DCAM-YOLOv5 in GPR B-Scan

Dejun CHEN¹, Shasha XIONG¹, Li GUO²

¹ School of Information Engineering, Wuhan University of Technology, Wuhan, 430079, China

² Wuhan Electric Power Technical College, Wuhan, 430079, China

872387122@qq.com, mrchendj@163.com

Submitted March 13, 2023 / Accepted May 17, 2023 / Online first May 23, 2023

Abstract. *This paper presents a detection method of DCAM-YOLOv5 for ground penetrating radar (GPR) to address the difficulty of identifying complex and multi-type defects in tunnel linings. The diversity of tunnel-lining defects and the multiple reflections and scattering caused by water-bearing defects make GPR images quite complex. Although existing methods can identify the position of underground defects from B-scans, their classification accuracy is not high. The DCAM-YOLOv5 adopts YOLOv5 as the baseline model and integrates deformable convolution and convolutional block attention module (CBAM) without adding a large number of parameters to improve the adaptive learning ability for irregular geometric shapes and boundary fuzzy defects. In this study, dielectric constant models of tunnel linings are established based on the electromagnetic simulation software (GPRMAX), including rebar and various structural defects. The simulated and field GPR B-scan images show that the DCAM-YOLOv5 method has better results for detecting different types of defects than other methods, which validates the effectiveness of the proposed detection method.*

Keywords

Ground penetrating radar, tunnel-lining defects, YOLOv5, deformable convolution, CBAM, GPRMAX

1. Introduction

The tunnel lining is a crucial component of tunnel engineering. However, they have been affected by geological conditions, leading to various underground defects such as cracks, voids, and delamination. These defects not only result in the gradual deterioration of tunnel structures but also pose a significant risk to safety of tunnels, such as instability and partial collapse, threatening the safe operation of tunnels [1], [2]. In addition, rebars in tunnel linings is an important component that carry the pressure and load of the entire tunnel structure. Any issues with rebars may cause linings to crack, deform, and affect the service life of tunnels [3], [4].

Ground penetrating radar (GPR) is an efficient, anti-interference, and highly penetrating non-destructive testing tool that provides more security and scientific support for underground engineering [5]. By emitting electromagnetic waves and receiving reflection signals, the GPR can form B-scan profiles and analyze underground defects in tunnel linings, inferring the location, shape, and type of defects [6], [7]. In tunnel lining inspection, traditional empirical interpretation of GPR images is time-consuming and prone to errors, resulting in poor inspection quality [8]. To improve tunnel safety and reduce inspection costs, the automated detection has become an important means of infrastructure inspection and is gradually becoming a future development trend [9], [10].

In GPR B-scans, cylindrical scatterers (such as rebars, pipelines, or circular voids) typically exhibit hyperbolic reflection characteristics. Hough transform is a common method for detecting hyperbolas in GPR B-scans [11–13]. However, the Hough transform is computationally expensive. To reduce computational cost, some researchers have used template matching and edge detection to fit hyperbolas in GPR B-scans [14], [15]. However, these methods typically only apply to identify hyperbolas with relatively regular reflection signals. In practical tunnel lining inspection, underground defects often exhibit irregular geometric shapes and present complex and irregular reflection curves in GPR B-scans [16].

With the rapid development of artificial intelligence, the automatic identification and analysis of GPR data has become a hot research topic. Kim et al. [17] proposed a road defect recognition method based on a convolutional neural network (CNN), which uses CNN to locate road defects after GPR image thresholding. Park [18] studied the performance of the YOLOv3 algorithm in real-time prediction of rebar diameters in facilities, and the result showed that the method can achieve real-time prediction. Yang et al. [19] showed that YOLOv5l can achieve the highest detection accuracy and effectively detected the coal fire range, providing a basis for coal fire disaster control. In addition, Li [20] compared the performance of YOLO series models in identifying and locating hidden cracks. Through the construction of a dataset

and detection experiments of the model, it was found that the method can accurately distinguish hidden cracks from false cracks. Chen [21] used the MobileNetV3-Large-CBAM model to process imbalanced datasets and hard samples, and performed well in bridge crack classification and identification. Huang [22] proposed an improved YOLO object detection algorithm based on the deformable convolution, which allows the network to adaptively learn the receptive field of feature points, thereby extracting more effective features for objects of different sizes and shapes and improving detection accuracy.

The success of deep learning models in the field of the GPR recognition suggests that identifying target objects from B-scans will become a future development trend. However, the diversity of tunnel-lining defects and the multiple reflections and scattering caused by water-bearing defects make the recorded GPR images quite complex. Although existing methods can identify the position of underground defects from B-scans, their classification accuracy is not high. To address the challenge of accurately identifying tunnel-lining defects, this study proposes a DCAM-YOLOv5 recognition method, which enhances the adaptability to complex geometric defects by designing the DBS module that can adaptively change according to the shape of defects. In addition, the introduction of the CBAM module improves the recognition accuracy of defects with unclear boundaries in GPR B-scans, enabling accurate identification of the position and type of tunnel-lining defects. Finally, the paper conducts numerical simulation experiments and field tests, and analyzed and verified the identification results of underground defect positions and types from GPR B-scans.

In this paper, the defect identification of irregular geometry was studied in depth. Our method achieves a precision of 90.81%, which is the best accuracy reported among all methods, beating the best (YOLO model) previous precision by 12.24%. The remaining sections of this paper are organized as follows: Section 2 describes the dataset used in this study, Section 3 presents the construction method of the DCAM-YOLOv5 defect detection model, Section 4 introduces and analyzes the experimental results, and finally, Section 5 summarizes the contributions and draws certain conclusions.

2. Construction of Tunnel Lining Underground Defect Dataset

2.1 Synthetic GPR B-Scans

Underground defects in tunnel linings include rebars and various types of defects such as cracks, voids, and delamination. These structural defects are further categorized into water-bearing and water-free defects according to their dielectric properties. In this study, the dielectric constants of water-free defects, water-bearing defects, and rebars are 1, 81, and 300, respectively. The dielectric constants of the lining

Forward simulation parameters	Specific configuration
Size of models [m]	1 × 2
Lining-rock interface [m]	0.2–0.5
Size of a spatial grid [m]	0.002
Time (ns)	20–30
Antenna step spacing [m]	0.1
Number of channels	170
Type of excitation source	Ricker
Frequency of excitation source [MHz]	400 600 900

Tab. 1. FDTD forward simulation parameters.

and surrounding rock are random and range from 6–7 and 8–10, respectively. Additionally, the interface between the lining and the surrounding rock is considered to be a rough and irregular surface. Based on the electromagnetic simulation software (GPRMAX), 2D dielectric constant models are developed to realistically simulate the internal structure of tunnel linings, with a size of 1 m × 2 m and finite difference time domain (FDTD) forward simulation parameters as shown in Tab. 1. Dielectric constant models maximally simulate the real situation of tunnel linings, including different combinations of single defects, multiple defects, and rebars, represented by different colors indicating water-free defects, water-bearing defects, and rebars. In the tunnel lining detection, GPR equipment with main frequencies of 400 MHz, 600 MHz, and 900 MHz are relatively common. Therefore, in this study, dielectric constant models were forward simulated using the FDTD method based on Ricker wavelet with main frequencies of 400 MHz, 600 MHz, and 900 MHz, to obtain synthetic GPR data with 170 channels. To increase the diversity of data and enhance the adaptability of the network, a total of 2400 synthetic GPR data with different frequencies and conductivities were generated. Figure 1 illustrates dielectric constant models and the corresponding synthetic GPR B-scans before and after removing the direct wave. For the code of the forward model, we have uploaded it to Github at <https://github.com/Crystal33-all/GPR>.

2.2 Field GPR B-Scans

In order to verify the applicability of the proposed method in practical situations, an on-site survey was conducted using the Italian RIS radar. In this experiment, the GPR device had a main frequency of 900 MHz, 512 sampling points, and a 0.01 m spacing between traces. Experimental walls were used to simulate the internal structure of tunnel linings, where water-free boxes and water-bearing boxes used to simulate water-free voids and water-bearing voids inside tunnel linings. In addition, steel meshes with different densities was deployed at different horizontal and depth positions on the experimental wall to increase the diversity of field GPR data.

Unlike synthetic GPR data, field GPR signals inevitably contain noise due to the heterogeneity of the subsurface medium, mutual wave interactions, and external conditions during data acquisition. Therefore, preprocessing techniques such as zero-offset correction, direct coupling removal,

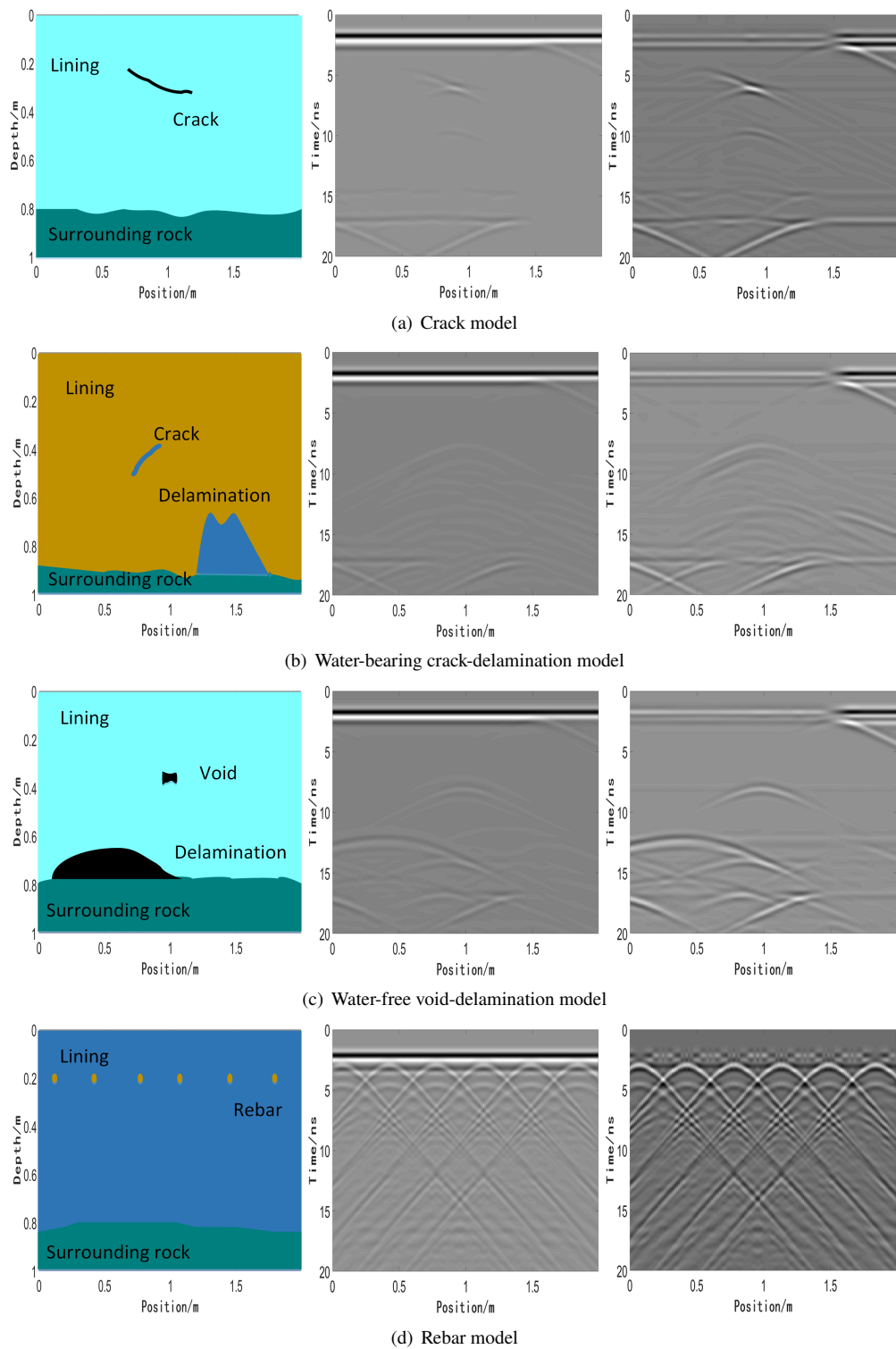


Fig. 1. Dielectric constant models and the corresponding synthetic GPR B-scans before and after removing the direct wave.

automatic gain, and clutter suppression are required to visualize and enhance these data. After a series of preprocessing techniques, field GPR data were obtained at a depth of 10 ns and a horizontal direction of 2 m. Their morphological patterns differ in terms of anomalous objects and complex geological structures, and a total of 316 field GPR data were obtained, including various reflection signals representing rebars and various structural defects (including voids and water-bearing voids). The synthetic GPR data in this paper and the field GPR data collected through the Italian RIS are referred to as the RGPR dataset.

The URIGPRv1.0 dataset contains easily detectable sample images from with the low level of areas, resulting in GPR images with minimal anomalies, as well as more challenging samples from areas with significant deterioration in bridge deck height, resulting in GPR images with low contrast and difficult-to-detect reflection hyperbolas [7]. The Warren County Bridge dataset was collected by Kaur [23] using GSSI SIR-20 GPR. Irenexychen [24] used data provided by Sensors and Software Inc. The GPR-SD dataset [25], [26] consists of GPR B-scan images collected by Zhou and Wang along cement and asphalt roads.

In this paper, five datasets were used to form the DEFECT dataset, which include the URIGPRv1.0 dataset, GPR-SD dataset, Warren County Bridge dataset, Irenexychen dataset, as well as the RGPR dataset presented in this paper.

3. Construction of DCAM-YOLOv5 Defect Detection Model

3.1 YOLOv5 Object Detection Model

YOLOv5 is an efficient, fast, and accurate detection algorithm that has gained increasing attention due to its outstanding performance and real-time detection capability. Since its release, YOLOv5 has been updated several times, and the paper selects the latest version 6.0 for research purposes. YOLOv5 can be divided into five different network models based on the depth and number of parameters in the model. Considering the trade-off between model size and accuracy, the paper chooses YOLOv5l as the baseline model for network improvement.

The YOLOv5l network consists of four parts: input, backbone, neck, and head, as shown in Fig. 2. The backbone network consists of CBS (Conv-BN-SiLU), C3, and SPPF modules. The version 6.0 and above have replaced the Focus module with an equivalent CBS module. The CBS module is composed of a convolutional layer, batch normalization layer, and SiLU activation function layer, aimed at extracting features. The neck network adopts the feature pyramid structure of FPN+PAN for multi-scale fusion. FPN realizes the transmission of high-to-low semantic information, while PAN realizes the transmission of low-to-high localization information.

3.2 Design of Deformable Convolutional Module

Due to various geometric shapes of defects and different materials in tunnel linings, the reflected signals in GPR B-scans exhibit significant irregularity and diversity. In addition, there exist unpredictable interference noises in the acquired GPR data, which further increases the complexity and diversity of the reflected signals in the GPR B-scan. YOLOv5 does not take geometric deformations into account when extracting features because traditional convolution operations fix their geometric structure, making the geometry of their stacked convolutional networks fixed as well, thus limiting the recognition ability of the model for objects with large degrees of geometric deformation. To address this issue, this paper adopts the modulated deformable convolution to better extract image features.

The standard convolution operation consists of two steps: first, sampling is performed on the input feature map using a regular grid R to obtain a set of sampling points; second, the convolution kernel is used to perform weighted calculations on these sampling points to obtain the convolution result. The size and dilation rate of the regular grid R define the receptive field size of the convolution kernel. Equation (1) defines a convolution kernel with a size of 3×3 and a dilation rate of 1:

$$R = \{(-1, -1), (-1, 0), \dots, (0, 1), (1, 1)\}. \quad (1)$$

For each position p_0 on the output feature map:

$$y(p_0) = \sum_{p_n \in R} \omega(p_n) \times x(p_0 + p_n) \quad (2)$$

where p_n enumerates the positions in R . In the operation of deformable convolution, an additional offset $\{\Delta p_n | n = 1, 2, \dots, N\}$, $N = |R|$ is added to the regular grid R . At the same time, a weight Δm_n is predicted for each sampling point, which results in the deformable convolution formula:

$$y(p_0) = \sum_{p_n \in R} \omega(p_n) \times x(p_0 + p_n + \Delta p_n) \times \Delta m_n. \quad (3)$$

The paper introduces the deformable convolution into the backbone network of YOLOv5l to enhance geometric deformation feature extraction capability. Since 1×1 deformable convolution does not have the ability to change the receptive field and suffers from instability in computing sampling point offsets, this article focuses on the 3×3 deformable convolution. To avoid overfitting, the batch normalization and the SiLU activation function are added to the deformable convolution. Specifically, this article replaces the standard convolution in the third and fourth CBS modules of the YOLOv5 backbone network with the same size deformable convolution to form the DBS module (see Fig. 3 for details). This designed backbone network can better extract geometric features and help to accurately detect targets.

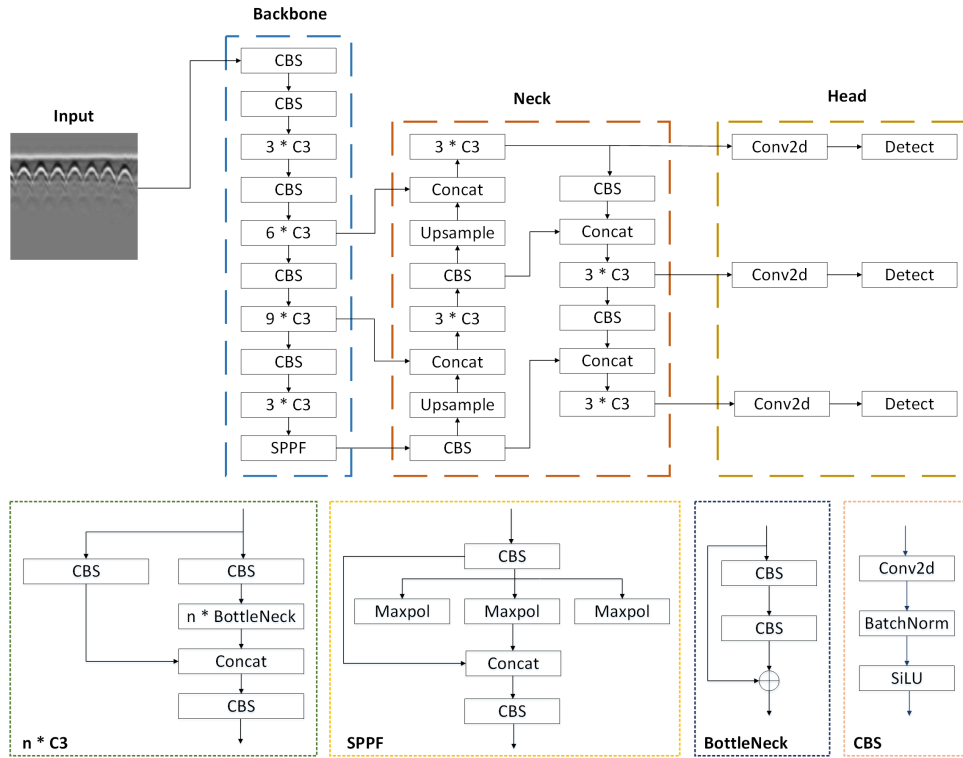


Fig. 2. The network architecture of YOLOv5l.

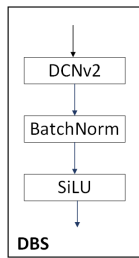


Fig. 3. The structure of the DBS module.

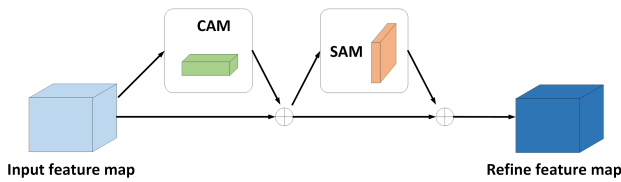


Fig. 4. The structure of the CBAM module.

3.3 Design of CBAM Module

Target reflection curves in the GPR B-scan are often obscure and there may be multiple targets with different geometries at the same level or depth. As the hyperbolic reflection patterns of these targets tend to overlap, along with the presence of a large amount of background clutter, it is difficult to distinguish subsurface infestations from the background. Therefore, it is extremely important to classify and identify the details of reflection curves in complex backgrounds.

After feature extraction by convolutional networks, a large amount of redundant information is introduced, leading to mislocalisation of the target boundary and resulting in loss of detection accuracy. To solve this problem, the Convolutional Block Attention Module (CBAM) is introduced in the YOLOv5 model, which is able to better represent the detail content through attention extraction of weights at different locations.

The CBAM was proposed by Woo [27] in 2018, and its core idea is to capture information interactions on different channels and spaces by computing Channel Attention Module (CAM) and Spatial Attention Module (SAM), as shown in Fig. 4.

The CAM generates a weight vector by calculating the difference between the mean and maximum values of the input tensor for each channel, and then applies this weight vector to the input tensor, weighting the different channels. The CAM can be expressed as:

$$M_c = \frac{1}{H \times W} \sum_{i=1}^H \sum_{j=1}^W x_{i,j,c}, \quad (4)$$

$$F_c = \sigma(MLP_{F_c}(M)) \quad (5)$$

where M_c represents the mean of the c channel and F_c represents the attention tensor of the channel after processing by the MLP layer and the Sigmoid activation function.

The SAM module generates a weight vector by calculating the mean and maximum values of each channel of the input tensor and then applies this weight vector to the input tensor, weighting the different spatial positions. The SAM can be expressed as:

$$M_s = \frac{1}{C} \sum_{c=1}^C x_{i,j,c}, \tag{6}$$

$$F_s = \sigma(MLP_{Conv}(M)) \tag{7}$$

where M_s represents the pixel average of all channels, and F_s represents the spatial attention tensor after the MLP layer and Sigmoid activation function.

The output of the CAM and the SAM module will be multiplied together to produce the final CBAM module output:

$$CBAM(x) = x \cdot (W_c \cdot F_c(x) \otimes W_s \cdot F_s(x)) \tag{8}$$

where W_c and F_c are learnable weight matrices.

In target detection tasks, different scale feature maps have different contributions to the performance and accuracy of the model. In general, small-scale feature maps contain more low-level features, medium-scale feature maps contain more contextual information, and large-scale feature maps contain more high-level features. Therefore, to make the model pay more attention to important features and reduce the interference of redundant information, the CBAM module can be used to optimize the feature maps at different scales.

Adding the CBAM module to the different feature maps of the YOLOv5 model maximizes its optimization effect and make the model more flexible to adapt to different target shapes and scales. At the same time, adding the CBAM to

the neck avoids compromising the speed and efficiency of the model. As the smaller the feature map, the faster the processing speed. Therefore, adding three CBAM modules to the neck of the YOLOv5 model can improve model performance and accuracy.

3.4 Design of DCAM-YOLOv5 Model

The YOLOv5l model performs very well in object detection, achieving high levels of detection accuracy and efficiency. However, it was designed based on conventional natural image detection and did not consider the geometric variability and background complexity of targets. Therefore, the paper proposes an improved YOLOv5 model structure by combining the design contents in Sec. 3.2 and Sec. 3.3, to better suit the detection of underground defects in tunnel linings. Figure 5 shows the network structure of DCAM-YOLOv5, with the improved parts highlighted in yellow and blue boxes. Some convolutional modules in backbone network are replaced by deformable convolutional modules (DCNv2+BN+SiLU, DBS), the core of which is to replace Conv in the convolutional module with a deformable convolution with modulation mechanism (DCNv2). The DBS module adaptively learns the geometrical variability of subsurface diseases, thus enhancing the model’s ability to extract multi-morphological target features. CBAMs are introduced into the neckbone network to extract attention to weights at different locations with a small number of additional parameters, thus weakening the interference of the noisy background and allowing the model to focus more on subsurface diseases. The introduction of these modules increases the geometric deformation feature extraction capability of DCAM-YOLOv5, enhances the model’s response to important spatial locations and suppresses the response to unimportant spatial locations, making it more flexible to adapt to different types of disease identification tasks.

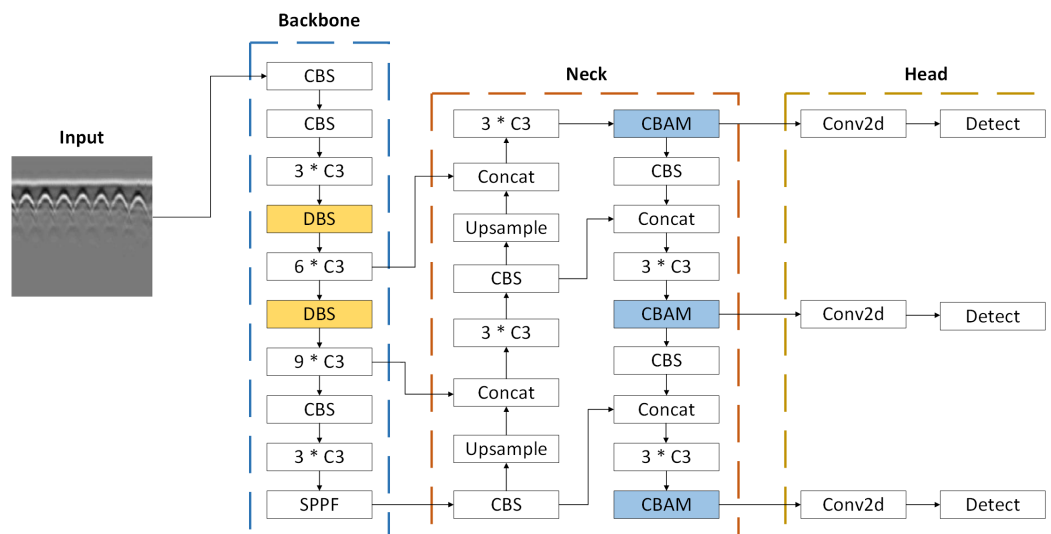


Fig. 5. The network structure of DCAM-YOLOv5.

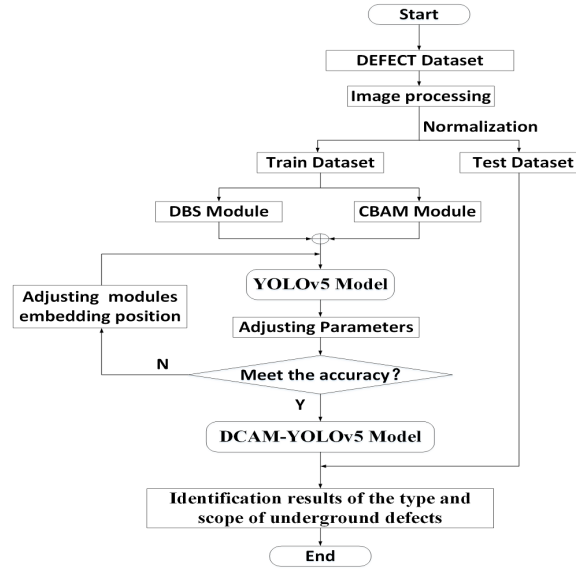


Fig. 6. The complete process of defect detection based on DCAM-YOLOv5.

Experimental platform	Hardware equipment	CPU	Intel 8700K
		GPU	GeForce GTX 1050Ti
		Memory	16G
		Hard disk	256G SSD + 1T HDD
	Software equipment	Graphics card	4G
		Operating system	Ubuntu 16.04
Model training parameters		CUDA version	9
		cuDNN version	7.14
		Framework	PyTorch
		Development library	Anaconda
		Programming language	Python 3.8
		Initial learning rate	1.0e-4
		Batch size	1

Tab. 2. Experimental environment configuration.

Figure 6 illustrates the complete process of defect detection based on DCAM-YOLOv5. Firstly, the DEFECT dataset needs to be preprocessed to highlight target reflection signals of GPR B-scans, including zero-point correction, direct wave removal, automatic gain control, and clutter suppression. Secondly, the preprocessed dataset is normalized and randomly divided into training and testing datasets in a 7 : 3 ratio. Then, the DBS and CBAM modules are embedded into the YOLOv5 model, and training parameters, including the initial learning rate, batch size, and number of iterations, are set based on the configuration of the network structure. If the accuracy requirement is satisfied, the trained DCAM-YOLOv5 model can be obtained; otherwise, the position of modules embedded in YOLOv5 will be further adjusted until the DCAM-YOLOv5 model that meets the accuracy requirement is obtained. Finally, the detection capability of the DCAM-YOLOv5 model for identifying the types and ranges of underground defects is tested using untrained field GPR data, realizing automatic detection of underground defects in tunnel linings.

In this paper, Intel 8700K CPU and single GeForce GTX 1050Ti graphics card are used as the main platform for algorithm implementation, and PyTorch deep learning framework is used to discuss the optimization of DCAM-YOLOv5 network architecture. At the same time, NVIDIA GPU drivers, CUDA and cuDNN environments are used to achieve GPU acceleration, thus improving training batches and accelerating training speed. Detailed information on the configuration of the specific experimental environment is shown in Tab. 2.

4. Results on Detection Performance Based on DCAM-YOLOv5

4.1 Performance Evaluation

In order to demonstrate that the DCAM-YOLOv5 detect model performs well, precision, recall, F1-score, and mean Average Precision (mAP) are used to compare and analyze detect results of four models. They are defined below:

$$Precision = \frac{TP}{TP + FP}, \tag{9}$$

$$Recall = \frac{TP}{TP + FN}, \tag{10}$$

$$F1-Score = 2 \times \frac{Precision \times Recall}{Precision + Recall}, \tag{11}$$

$$mAP = \frac{1}{n} \sum_{i=1}^n AP_i \tag{12}$$

where TP represents the number of true positives, FP represents the number of false positives, FN represents the number of false negatives, and n represents the number of categories. True positives refer to the number of samples that the classifier correctly predicts as positive samples, false positives refer to the number of samples that the classifier incorrectly predicts as positive samples from negative samples, and false negatives refer to the number of samples that the classifier incorrectly predicts as negative samples from positive samples.

4.2 Simulation Data Detection Results

Figure 7 presents the training results of DCAM-YOLOv5 and its variant architectures on GPR B-scans for various types of defects. DCN-YOLOv5 refers to the YOLOv5 structure with added deformable convolution (DCN) modules, while CBAM-YOLOv5 refers to the YOLOv5 structure with added CBAM module. As can be seen from Fig. 7(a), the final loss of the DCAM-YOLOv5 model is less than 0.05, while the final loss of the other three models ranges from 0.05 to 0.1. The combined loss and mAP show that DCAM-YOLOv5 outperforms the other three models, and the gradient propagation is more stable, with no significant fluctuations in the numerical curves, indicating that the DCAM-YOLOv5 model fits tunnel-lining defects dataset better.

Compared to YOLOv5, DCN-YOLOv5 achieves performance gains of 1.88% and 4.03% in F1-Score and mAP respectively. In addition, adding CBAMs to YOLOv5 also improved mAP by 1.58% and precision by 2.45%. This confirms that both strong feature representation and attention mechanism capabilities contribute to improved detection of complex GPR images. According to Tab. 3, compared to DCN-YOLOv5 and CBAM-YOLOv5, DCAM-YOLOv5 has a great improvement in each index, with an increase of 2.03% and 1.64% respectively in mAP, indicating that the DCAM-YOLOv5 model can identify different categories of defects and for each class of defects were identified relatively well.

The classification results of the DCAM-YOLOv5 and its variant architecture models performed on the DEFECT dataset are shown in Tab. 4. YOLOv5 achieved acceptable results and made very accurate predictions of voids, delamination and rebars. The loss function of YOLOv5 focuses on probabilities per pixel, but is limited to the overall effect, which results in lower resolution, making it difficult to identify small target defects. As a result, it performs poorly on cracks and has the lowest precision. The identification of cracks requires high resolution, which is even more difficult for the identification problem. Secondly, GPR data is more complex when multiple defects occur at different depths at the same location. CBAM-YOLOv5 struggles to effectively classify defects, particularly cracks and water-bearing delamination. DCN-YOLOv5 outperforms CBAM-YOLOv5 in terms of detection and can accurately identify defects with different geometries, but the effect of water-bearing voids of DCN-YOLOv5 is very poor. This is because the scattering of water-bearing voids generates multiple waves, which can easily lead to erroneous or redundant object detection frames by DCN-YOLOv5.

Models	Precision [%]	Recall [%]	F1-score	mAP@0.5 [%]
YOLOv5	78.57	77.43	0.7787	84.56
DCN-YOLOv5	86.46	85.54	0.8537	88.49
CBAM-YOLOv5	82.96	84.31	0.8416	87.62
DCAM-YOLOv5	90.81	87.69	0.8917	90.07

Tab. 3. Comparison of evaluation metrics for different models.

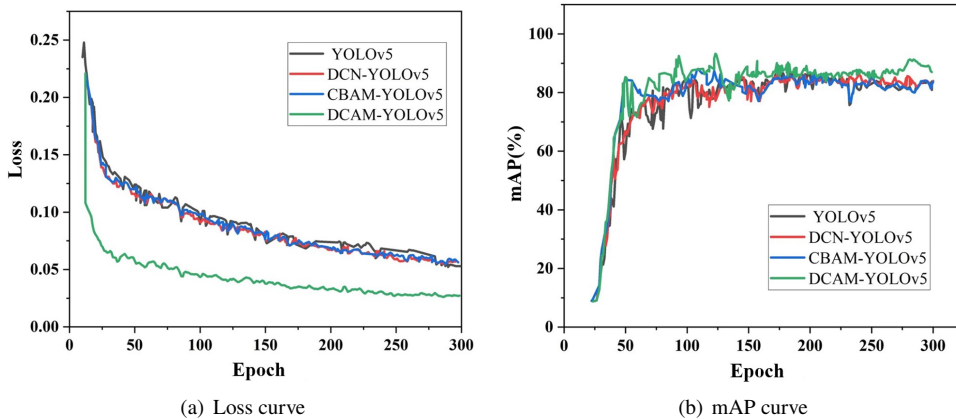


Fig. 7. The training results of different models.

Evaluations	Models	Rebar	Water-free defects			Water-bearing defects		
			Crack	Void	Delamination	Crack	Void	Delamination
Precision [%]	YOLOv5	95.67	48.48	79.08	81.21	81.10	69.65	77.11
	DCN-YOLOv5	98.43	83.24	81.09	89.18	86.19	78.07	86.19
	CBAM-YOLOv5	93.12	51.08	86.74	90.19	87.54	84.41	87.54
	DCAM-YOLOv5	99.64	91.25	92.08	95.11	88.33	84.78	89.98
Recall [%]	YOLOv5	91.45	62.11	75.36	84.91	79.89	74.96	75.15
	DCN-YOLOv5	97.69	84.95	80.01	87.30	85.29	76.29	85.29
	CBAM-YOLOv5	92.01	68.89	83.35	89.23	87.03	83.79	87.03
	DCAM-YOLOv5	97.41	83.39	88.69	89.60	87.40	84.03	87.15
F1-score	YOLOv5	0.9358	0.5446	0.7718	0.8302	0.8049	0.7221	0.7612
	DCN-YOLOv5	0.9806	0.8409	0.8054	0.8823	0.8574	0.7717	0.8574
	CBAM-YOLOv5	0.9256	0.5866	0.8501	0.8971	0.8728	0.8410	0.8728
	DCAM-YOLOv5	0.9851	0.8714	0.9035	0.9227	0.8786	0.8440	0.8859
mAP@0.5 [%]	YOLOv5	92.56	50.75	83.13	85.54	76.85	62.95	77.23
	DCN-YOLOv5	94.95	87.33	85.86	87.56	85.26	80.54	84.12
	CBAM-YOLOv5	92.01	76.48	89.41	88.51	86.10	79.63	83.15
	DCAM-YOLOv5	99.02	93.86	90.90	91.56	87.15	85.03	87.86

Tab. 4. Performance of different models in identifying different categories of defects.

Comparing all data in Tab. 4, it is easy to see that DCAM-YOLOv5 performs the best performance among all defects. It accurately predicts the location and type of cracks, voids and delamination and proves to be suitable for detecting reflective signals of any complex pattern in tunnel linings. Good results can be obtained for smaller target defects such as cracks and rebars. In general, most predicted results are accurate. The presence of water-bearing may cause some results to be incorrect, but the probability of error is very low. This result demonstrates the validity of the proposed method.

Figures 8 and 9 demonstrate the recognition results of YOLOv5, DCN-YOLOv5, CBAM-YOLOv5, and DCAM-YOLOv5 on simulated GPR B-scans, respectively. According to Figs. 8 and 9, (a) shows tunnel-lining models with a single defect, (b), (c), (d) and (e) show recognition results of YOLOv5, DCN-YOLOv5, CBAM-YOLOv5, respectively. As shown in Fig. 8(b), YOLOv5 can effectively recognize voids, delamination, and rebars, but it fails to identify small target cracks. According to Fig. 8(c) and (d), both DCN-YOLOv5 and CBAM-YOLOv5 can locate single defect in GPR B-scans and accurately identify the type of defects. CBAM-YOLOv5 demonstrates high confidence in recognizing different types of defects, while DCN-YOLOv5 can increase the receptive field and achieve precise defect localization. These observation results suggest that the deformable convolution module providing accurate location and the CBAM extracting shape features can collectively improve the ability to detect various single and irregularly shaped defects in tunnel linings.

According to Fig. 9, it can be seen that DCAM-YOLOv5 can accurately locate all defects in GPR B-scans, while the detection results generated by the other three methods are relatively poor. As shown in the first column of Fig. 9, when two defects are located at different depths in the same position, YOLOv5 can only recognize larger voids compared to

the crack, and CBAM-YOLOv5 has inaccurate positioning for water-bearing voids. As shown in the second column of Fig. 9, all four models have strong recognition ability for regular rebars. From the third column of Fig. 9, DCN-YOLOv5 is prone to identify noise as cracks, while YOLOv5 and CBAM-YOLOv5 may ignore shallow targets and treat them as noise, which may result in missing, redundant, or erroneous object detection boxes.

In summary, algorithms such as YOLOv5, DCN-YOLOv5 and CBAM-YOLOv5 have been used in this paper to detect defects in tunnel linings. However, these algorithms suffer from a number of problems, such as the inability to identify complex morphological defects, incorrect type identification and inaccurate location of defects. In contrast, the DCAM-YOLOv5 shows good performance in identifying multiple defects and performs well in the case of identifying multiple defects, which is especially suitable for detecting multiple defects with complex and irregular shapes in tunnel linings.

4.3 Application to Field GPR Datas

The DCAM-YOLOv5 has demonstrated excellent adaptability in GPR B-scans obtained through forward simulation experiments. To validate the applicability of the proposed method in engineering, the DCAM-YOLOv5 was applied to automatically detect reflection signals in GPR images obtained from measurements of multiple tunnels. The recognition results, as shown in Fig. 10, indicate that DCAM-YOLOv5 can accurately identify the location and type of concealed defects in tunnel linings, especially for small targets such as deep voids and water-bearing cracks. Therefore, the DCAM-YOLOv5 has good generalization ability and adaptability to different scenarios and task requirements, except for cases where reflection features are not clearly visible and cannot be recognized.

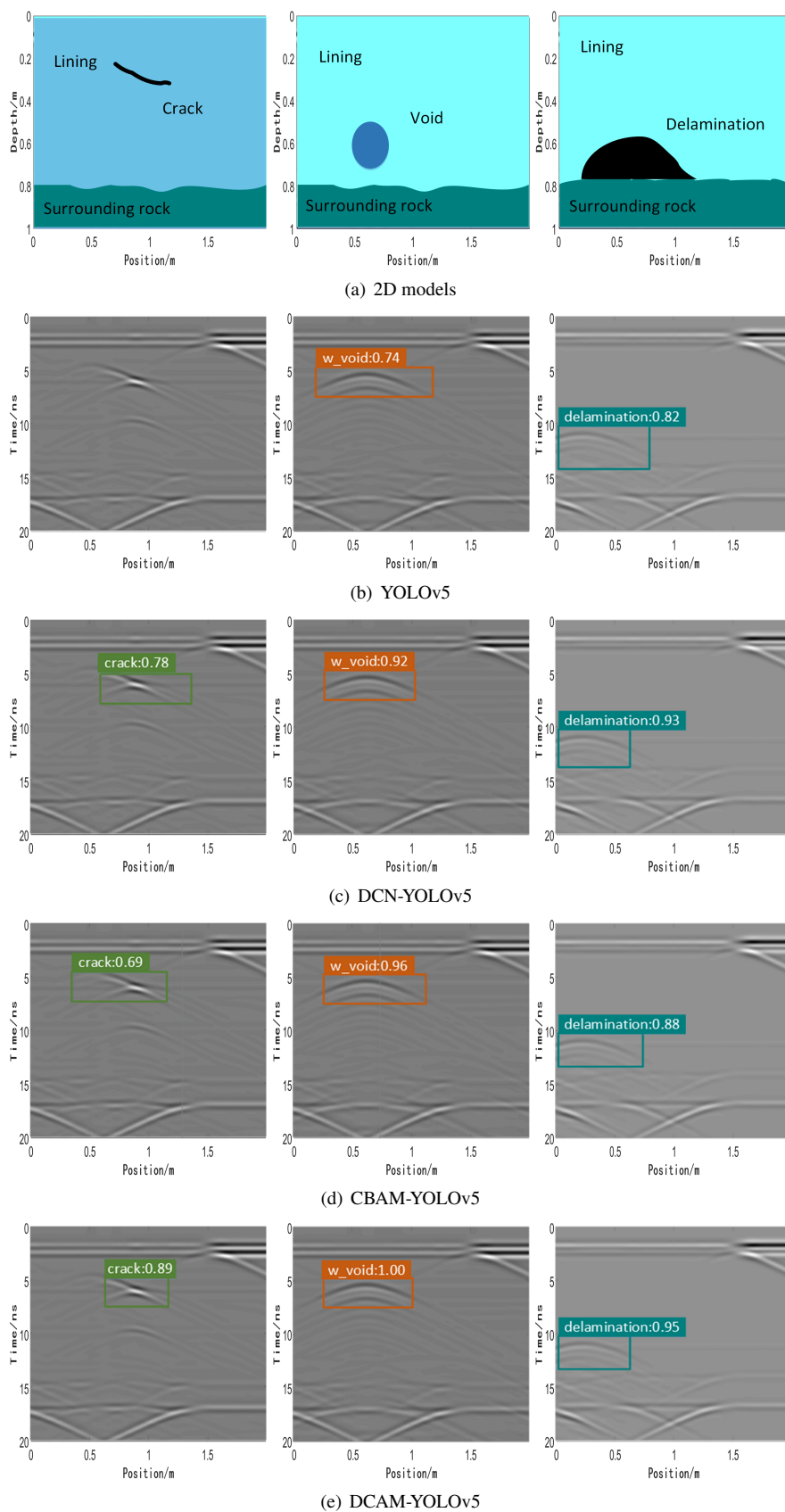


Fig. 8. The recognition single defect results of YOLOv5, DCN-YOLOv5, CBAM-YOLOv5, and DCAM-YOLOv5 on simulated GPR B-scans.

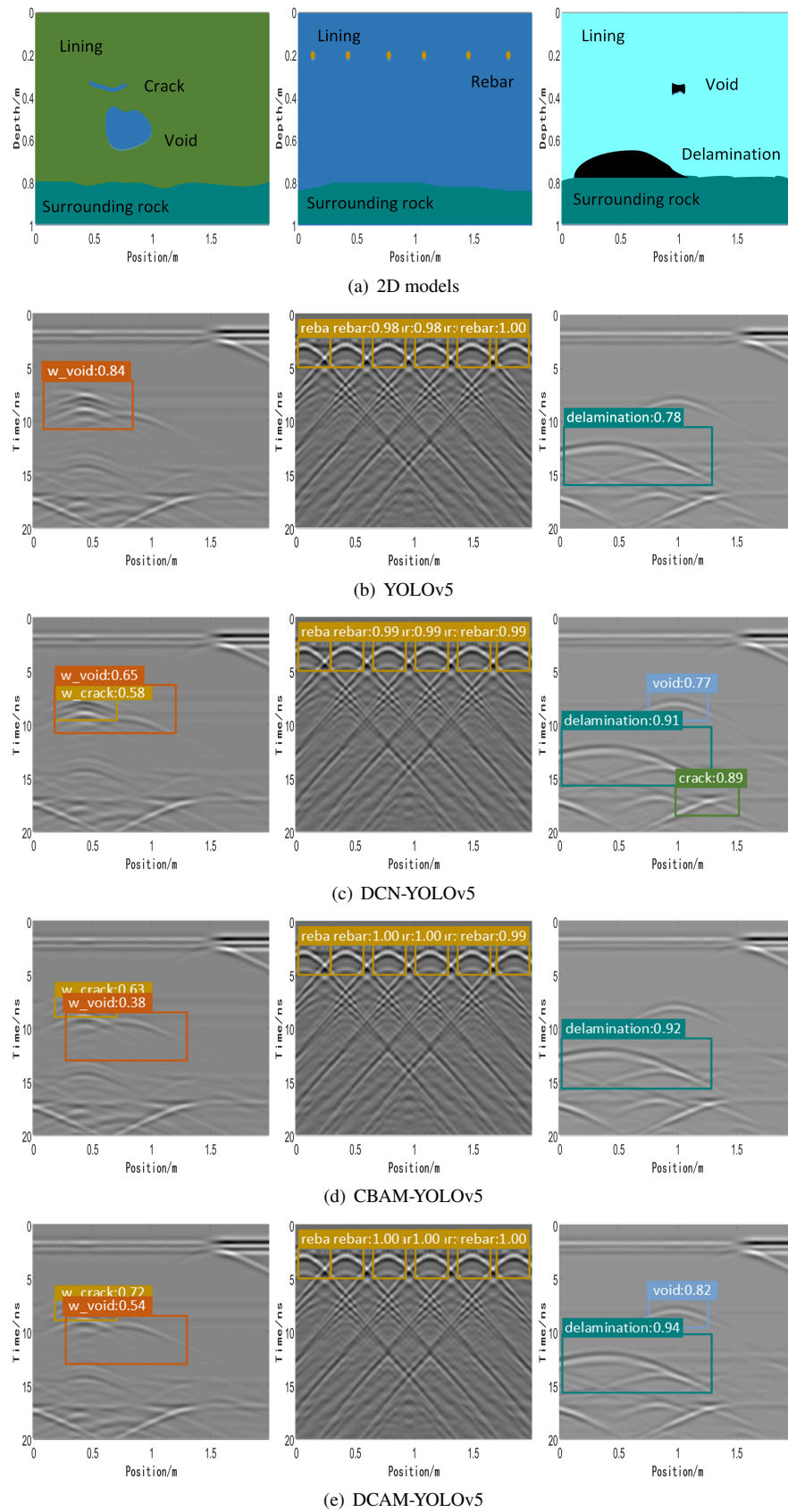


Fig. 9. The recognition multiple defects result of YOLOv5, DCN-YOLOv5, CBAM-YOLOv5, and DCAM-YOLOv5 on simulated GPR B-scans.

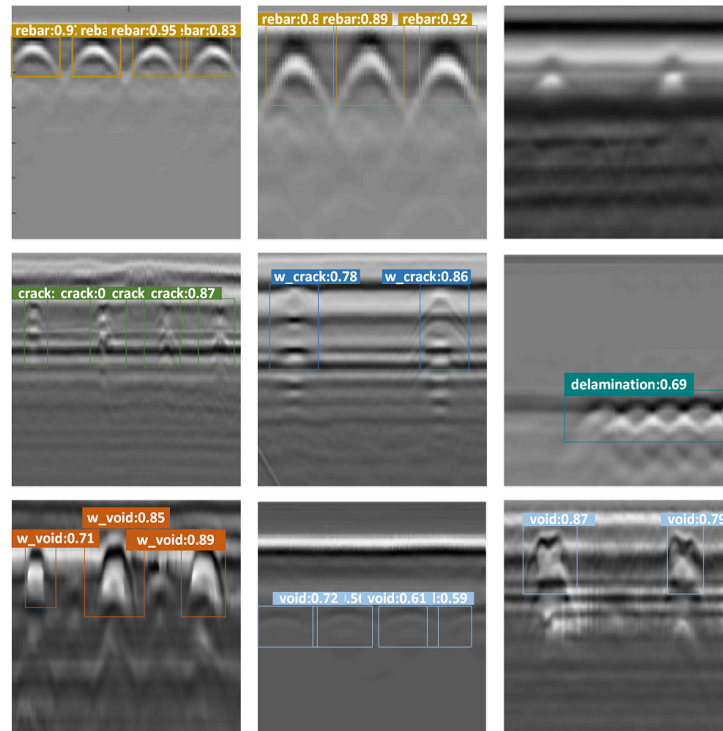


Fig. 10. Object detection results of CBAM-YOLOv5 applied on field GPR datas.

5. Conclusions

In this study, we proposed a DCAM-YOLOv5 method for GPR data to automatically detect underground defects in tunnel linings. Specifically, DBS modules were introduced to replace two convolutional blocks in the YOLOv5 backbone network, which enables the network to adaptively learn the receptive field of feature points and extract more effective features for objects of different sizes and shapes. Additionally, CBAMs were incorporated to improve the weight of important regions while keeping the model lightweight. Experimental results on the dataset constructed in this paper demonstrate that DCAM-YOLOv5 can effectively improve target detection accuracy and robustness, with mAP reaching 90.07%, a 5.51% increase compared to YOLOv5. Additionally, DCAM-YOLOv5 exhibited satisfactory results in field experiments, demonstrating its practical applicability for real-world tunnel inspections.

Although DCAM-YOLOv5 obtained suitable results when applied to synthetic and field GPR data, it had certain limitations on the diversity of field GPR. Therefore, future research needs to conduct further experiments on larger and more diverse sets of real GPR images to verify the system's actual application performance.

Acknowledgments

This work was supported by the Chinese Academy of Railway Science Foundation Project (1951JJ5703).

References

- [1] JIANG, Y. J., ZHANG, X. P., TANIGUCHI, T. Quantitative condition inspection and assessment of tunnel lining. *Automation in Construction*, 2019, vol. 102, p. 258–269. DOI: 10.1016/j.autcon.2019.03.001
- [2] YE, F., QIN, N., LIANG, X., et al. Analyses of the defects in highway tunnels in China. *Tunnelling and Underground Space Technology*, 2021, vol. 107, p. 1–17. DOI: 10.1016/j.tust.2020.103658
- [3] TESIC, K., BARICEVIC, A., SERDAR, M. Non-destructive corrosion inspection of reinforced concrete using ground-penetrating radar: A review. *Materials*, 2021, vol. 14, no. 4, p. 1–20. DOI: 10.3390/ma14040975
- [4] GOMEZA, J., CASAS, J. R., VILLALBA, S. Structural health monitoring with distributed optical fiber sensors of tunnel lining affected by nearby construction activity. *Automation in Construction*, 2020, vol. 117, p. 1–18. DOI: 10.1016/j.autcon.2020.103261
- [5] MURTHY, A. R., PUKAZHENDHI, D., VISHNUVARDHAN, S., et al. Performance of concrete beams reinforced with GFRP bars under monotonic loading. *Structures*, 2020, vol. 27, p. 1274–1288. DOI: 10.1016/j.istruc.2020.07.020
- [6] LEI, M. F., LIU, L. H., SHI, C. H., et al. A novel tunnel-lining crack recognition system based on digital image technology. *Tunnelling and Underground Space Technology*, 2021, vol. 108, p. 1–13. DOI: 10.1016/j.tust.2020.103724
- [7] ASADI, P., GINDY, M., ALVAREZ, M., et al. A computer vision based rebar detection chain for automatic processing of concrete bridge deck GPR data. *Automation in Construction*, 2020, vol. 112, p. 1–12. DOI: 10.1016/j.autcon.2020.103106
- [8] LOUPOS, K., DOULAMIS, A. D., STENTOUMIS, C., et al. Autonomous robotic system for tunnel structural inspection and assessment. *International Journal of Intelligent Robotics and Applications*, 2018, vol. 2, no. 1, p. 43–66. DOI: 10.1007/s41315-017-0031-9

- [9] OKAZAKI, Y., OKAZAKI, S., ASAMOTO, S., et al. Applicability of machine learning to a crack model in concrete bridges. *Computer-Aided Civil and Infrastructure Engineering*, 2020, vol. 35, no. 8, p. 775–792. DOI: 10.1111/mice.12532
- [10] LEI, W., HOU, F., XI, J., et al. Automatic hyperbola detection and fitting in GPR B-scan image. *Automation in Construction*, 2019, vol. 106, p. 1–14. DOI: 10.1016/j.autcon.2019.102839
- [11] TAKAHIRO, Y., TSUKASA, M. Detection and localization of man-hole and joint covers in radar images by support vector machine and Hough transform. *Automation in Construction*, 2021, vol. 126, p. 1–12. DOI: 10.1016/j.autcon.2021.103651
- [12] LEE, K. L., MOKJI, M. M. Automatic target detection in GPR images using histogram of oriented gradients (HOG). In *2nd International Conference on Electronic Design (ICED)*. Penang (Malaysia), 2014, p. 181–186. DOI: 10.1109/ICED.2014.7015795
- [13] NOREEN, T., KHAN, U. S. Using pattern recognition with HOG to automatically detect reflection hyperbolas in ground penetrating radar data. In *International Conference on Electrical and Computing Technologies and Applications (ICECTA)*. Ras Al Khaimah (United Arab Emirates), 2017, p. 1–6. DOI: 10.1109/ICECTA.2017.8252064
- [14] MERTENS, L., PERSICO, R., MATERA, L., et al. Automated detection of reflection hyperbolas in complex GPR images with no a priori knowledge on the medium. *IEEE Transactions on Geoscience and Remote Sensing*, 2016, vol. 54, no. 1, p. 580–596. DOI: 10.1109/TGRS.2015.2462727
- [15] PEER, U., DÝ, J. G. Automated target detection for geophysical applications. *IEEE Transactions on Geoscience and Remote Sensing*, 2017, vol. 55, no. 3, p. 1563–1572. DOI: 10.1109/TGRS.2016.2627245
- [16] ZHOU, Z., ZHANG, J., GONG, C. Automatic detection method of tunnel lining multi-defects via an enhanced you only look once network. *Computer-Aided Civil and Infrastructure Engineering*, 2022, vol. 37, no. 6, p. 762–780. DOI: 10.1111/mice.12836
- [17] KIM, N., KIM, K., AN, Y. K., et al. Deep learning-based underground object detection for urban road pavement. *International Journal of Pavement Engineering*, 2020, vol. 21, no. 13, p. 1638–1650. DOI: 10.1080/10298436.2018.1559317
- [18] PARK, S., KIM, J., JEON, K., et al. Improvement of GPR-based rebar diameter estimation using YOLO-v3. *Remote Sensing*, 2021, vol. 13, no. 10, p. 1–12. DOI: 10.3390/rs13102011
- [19] YANG, J., SONG, F. B., ZHANG, P. L., et al. Application of deep learning in ground penetrating radar image recognition. In *International Conference on Artificial Intelligence (CAIBDA)*. Xi'an (China), 2021, p. 16–20. DOI: 10.1109/CAIBDA53561.2021.00011
- [20] LI, S. W., GU, X. Y., XU, X. G., et al. Detection of concealed cracks from ground penetrating radar images based on deep learning algorithm. *Construction and Building Materials*, 2021, vol. 273, p. 1–14. DOI: 10.1016/j.conbuildmat.2020.121949
- [21] CHEN, L. J., YAO, H. D., FU, J. Y., et al. The classification and localization of crack using lightweight convolutional neural network with CBAM. *Engineering Structures*, 2023, vol. 275, no. B, p. 1–16. DOI: 10.1016/j.engstruct.2022.115291
- [22] HUANG, F. Q., CHEN, M., FENG, G. F. Improved YOLO object detection algorithm based on deformable convolution. (in Chinese). *Computer Engineering*, 2021, vol. 47, no. 10, p. 269–275, 282. DOI: 10.19678/j.issn.1000-3428.0059096
- [23] KAUR, P., DANA, K. J., ROMERO, F. A., et al. Automated GPR rebar analysis for robotic bridge deck evaluation. *IEEE Transactions on Cybernetics*, 2015, vol. 46, no. 10, p. 2265–2276. DOI: 10.1109/TCYB.2015.2474747
- [24] CHEN, I. X. Y. *GPR-Data-Classifier*. [Online]. Available at: <https://github.com/irenexychen/gpr-data-classifier>
- [25] ZHOU, X. R., CHEN, H. H., LI, J. L., et al. An automatic GPR B-scan image interpreting model. *IEEE Transactions on Geoscience and Remote Sensing*, 2018, vol. 56, no. 6, p. 3398–3412. DOI: 10.1109/TGRS.2018.2799586
- [26] WANG, X. Y., CHEN, L., BAN, T. Y., et al. Accurate label refinement from multiannotator of remote sensing data. *IEEE Transactions on Geoscience and Remote Sensing*, 2023, vol. 61, p. 1–13. DOI: 10.1109/TGRS.2023.3241402
- [27] WOO, S., PARK, J., LEE, J., et al. CBAM: Convolutional block attention module. In *Proceedings of the European conference on computer vision (ECCV)*. Munich (Germany), 2018, p. 3–19. DOI: 10.1007/978-3-030-01234-2_1

About the Authors ...

Dejun CHEN was born in 1964. He received his D.E. in 2003. His research interests include complex system modeling, distributed decision support systems, embedded systems.

Shasha XIONG (corresponding author) was born in 1997. Her research interests include signal processing and image processing.

Li GUO was born in 1981. His research interests include computer simulation, computer networks and communication.